

A Strong-Coupling-Limit Study on the Pairing Mechanism in the Pressurized $\text{La}_3\text{Ni}_2\text{O}_7$

Jia-Heng Ji,^{1,*} Chen Lu,^{2,*} Zhi-Yan Shao,^{1,*} Zhiming Pan,^{3,*} Fan Yang,^{1,†} and Congjun Wu^{4,5,6,7,‡}

¹*School of Physics, Beijing Institute of Technology, Beijing 100081, China*

²*School of Physics and Hangzhou Key Laboratory of Quantum Matter, Hangzhou Normal University, Hangzhou 311121, China*

³*Department of Physics, Xiamen University, Xiamen 361005, Fujian, China*

⁴*New Cornerstone Science Laboratory, Department of Physics,*

School of Science, Westlake University, Hangzhou 310024, Zhejiang, China

⁵*Institute for Theoretical Sciences, Westlake University, Hangzhou 310024, Zhejiang, China*

⁶*Key Laboratory for Quantum Materials of Zhejiang Province,*

School of Science, Westlake University, Hangzhou 310024, Zhejiang, China

⁷*Institute of Natural Sciences, Westlake Institute for Advanced Study, Hangzhou 310024, Zhejiang, China*

Recently, the bilayer perovskite nickelate $\text{La}_3\text{Ni}_2\text{O}_7$ has been reported to exhibit high-temperature superconductivity (SC) near 80K under a moderate pressure of about 14GPa. To investigate the underlying pairing mechanism and symmetry in this complex system, we propose and analyze a mixed spin-1 and spin- $\frac{1}{2}$ bilayer t - J model in the strong coupling regime. This model explicitly incorporates the crucial role of strong Hund's coupling, which favors the formation of local spin-triplet states from the two onsite E_g orbital electrons at half-filling. We further investigate the model using both slave-particle mean-field theory and the density matrix renormalization group method. Our simulation results reveal that the dominate pairing channel is the interlayer one in the $3d_{x^2-y^2}$ orbital. The Hund's coupling is shown to enhance SC within a reasonable physical range. Moreover, electron doping strengthens SC by increasing carrier density; in contrast, hole doping weakens SC. These findings offer critical insights into the unconventional SC of pressurized $\text{La}_3\text{Ni}_2\text{O}_7$ and underline the important role of orbital-selective behavior and Hund's rule.

I. INTRODUCTION

The discovery of high-temperature superconductivity (SC) in the bilayer perovskite nickelate $\text{La}_3\text{Ni}_2\text{O}_7$ under pressure [1–10] has garnered widespread attention, both experimentally [11–31] and theoretically [32–77]. More recently, the observation of ambient-pressure SC in thin-film samples has attracted further attention [78–84]. These findings highlight the potential of nickelates as a new platform for exploring unconventional superconductors, particularly as analogs to the extensively studied cuprates [85–89]. In cuprates, doping introduces holes into the oxygen $2p$ orbitals, which form Zhang-Rice singlets with localized $3d_{x^2-y^2}$ orbital spins in the Cu^{2+} ions [90]. The suppression of long-range antiferromagnetic (AFM) order under doping leads to d -wave SC [85, 86]. A similar scenario has been proposed for infinite-layer nickelates such as $\text{Nd}_{1-x}\text{Sr}_x\text{NiO}_2$ [91–93]. However, $\text{La}_3\text{Ni}_2\text{O}_7$ under pressure presents a more complex challenge due to its bilayer structure, unusual orbital filling, and strong electron correlations.

Recent theoretical and experimental studies have indicated that pressurized $\text{La}_3\text{Ni}_2\text{O}_7$ exhibits remarkable orbital-selective strong-correlation effects: According to first-principles calculations based on density-functional theory (DFT), the low-energy physics near the Fermi

level are dominated by Ni- $3d_{z^2}$ and Ni- $3d_{x^2-y^2}$ orbitals, with occupancies of approximately half and one-quarter, respectively [32, 36–38, 61–66]. A range of experiments have demonstrated the strongly-correlated characteristic of the bilayer nickelate material [13, 14, 19, 21, 22, 24–27]. For instance, optical measurements report a notable reduction in electron kinetic energy, indicating proximity to the Mott phase [22]; angle-resolved photoemission spectroscopy (ARPES) experiment reveals pronounced orbital-selective band renormalization [24]; linear temperature dependence of resistivity points to “strange-metal” behavior [2]; the transport measurements of resistivity and magneto-resistance confirm Kondo-like scattering [27]. Together, these findings suggest that $\text{La}_3\text{Ni}_2\text{O}_7$ under pressure may provide a novel platform for exploring the interplay between orbital selectivity, strong correlations, and Hund's coupling.

Presently, the pairing mechanism in the pressurized $\text{La}_3\text{Ni}_2\text{O}_7$ remains an open question due to its complex electronic nature [32–75, 77]. A key issue among theoretical proposals is determining which orbitals are most relevant for the SC. Some perspectives suggest that the SC of pressurized $\text{La}_3\text{Ni}_2\text{O}_7$ is significantly related to hybridization between the nearest-neighbor (NN) $3d_{z^2}$ and $3d_{x^2-y^2}$ orbitals [39–41, 67–72], while others emphasize the critical role of Hund's coupling in driving the superconducting behavior [35, 46, 48, 54, 55, 57–59, 67, 69, 71–73]. There is also a possibility that both factors are involved.

In this work, we propose and study a mixed spin-1 and spin- $\frac{1}{2}$ bilayer E_g -orbital t - J model, incorporating the

* These four authors contributed equally to this work.

† yangfan_blg@bit.edu.cn

‡ wucongjun@westlake.edu.cn

spin coupling between the two orbitals. This model establishes a strong-coupling framework for identifying the dominant pairing channel in the bilayer system, while explicitly linking Hund's rule to superconducting strength with the preservation of the hole configuration. We solve the ground state using slave-particle mean-field (SPMF) [86, 94] and the density matrix renormalization group (DMRG) [95, 96] methods. The numerical results reveal a phase diagram where the dominant pairing occurs in the interlayer $3d_{x^2-y^2}$ orbitals. The Hund's coupling J_H promotes SC pairing and attracts a few $3d_{z^2}$ -orbital electrons to the $3d_{x^2-y^2}$ -orbital. The effect of doping is further explored, where electron-doping will enhance the SC pairing.

II. EFFECTIVE BILAYER TWO-ORBITAL MODEL

The electronic characteristics of the bilayer $\text{La}_3\text{Ni}_2\text{O}_7$ under pressure are predominantly influenced by the $d_{x^2-y^2}$ and d_{z^2} orbitals within the NiO_2 planes, which are naively quarter-filling and half-filling, respectively. The $d_{x^2-y^2}$ orbital is primarily responsible for in-plane conduction and dominates the electronic states near the Fermi level, contributing to the metallic behavior observed in the normal state. On the other hand, the d_{z^2} orbital is more localized, with its lobes extending out of the NiO_2 planes, thereby mediating the interlayer coupling between adjacent NiO_2 planes and leads to the formation of bonding and anti-bonding states [1].

The electronic properties of the bilayer $\text{La}_3\text{Ni}_2\text{O}_7$ are described by a two-orbital Hubbard model on the bilayer square lattice given as $H_{\text{Hubbard}} = H_t + H_{\text{Int}}$. Here, the kinetic part is given by

$$\begin{aligned}
H_t = & \sum_{i\mu\alpha\sigma} \epsilon_\alpha n_{i\mu\alpha\sigma} - \sum_{\langle ij \rangle \mu\sigma} t_{zz}^\parallel (c_{i\mu z\sigma}^\dagger c_{j\mu z\sigma} + \text{h.c.}) \\
& - \sum_{\langle ij \rangle \mu\sigma} t_{xx}^\parallel (c_{i\mu x\sigma}^\dagger c_{j\mu x\sigma} + \text{h.c.}) \\
& - \sum_{\langle ij \rangle \mu\sigma} t_{zx}^\parallel (c_{i\mu z\sigma}^\dagger c_{j\mu x\sigma} + (z \leftrightarrow x) + \text{h.c.}) \\
& - \sum_{i\sigma} t_{zz}^\perp (c_{it z\sigma}^\dagger c_{ib z\sigma} + \text{h.c.}),
\end{aligned} \tag{1}$$

where $c_{i\mu\alpha\sigma}^\dagger$ creates an $\alpha = \{d_{z^2}(z), d_{x^2-y^2}(x)\}$ -orbital electron with spin $\sigma = \{\uparrow, \downarrow\}$ at the lattice site i in the layer $\mu = \{\text{top}(t), \text{bottom}(b)\}$; $\langle ij \rangle$ represents the intralayer NN bonds; $t_{zz}^\parallel, t_{zx}^\parallel, t_{xx}^\parallel$ and t_{zz}^\perp are hopping integrals as shown in Fig. 1(a), of which t_{zx}^\parallel represents the non-zero NN hybridization between the two E_g orbitals, exhibiting opposite signs along x - and y -directions due to the symmetry constraint, $t_{zx,x}^\parallel = -t_{zx,y}^\parallel = t_{zx}^\parallel$; ϵ_α denotes the onsite energy for each orbital.

The interacting part for the two-orbital system is given

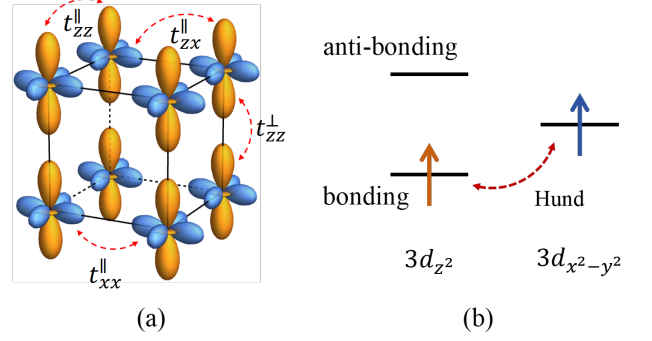


FIG. 1. (a) Two E_g orbitals in the bilayer structure of the nickelate $\text{La}_3\text{Ni}_2\text{O}_7$ with the relevant hopping integrals. (b) Under strong interlayer hybridization, the d_{z^2} -band splits into an interlayer bonding and anti-bonding bands, respectively. The bonding band is energetically favored. The d_{z^2} and $d_{x^2-y^2}$ electrons tend to form a spin triplet due to strong Hund's coupling.

by

$$\begin{aligned}
H_{\text{Int}} = & U \sum_{i\mu\alpha} n_{i\mu\alpha\uparrow} n_{i\mu\alpha\downarrow} + V \sum_{i\mu\sigma\sigma'} n_{i\mu z\sigma} n_{i\mu x\sigma'} \\
& - 2J_H \sum_{i\mu} \left(\mathbf{S}_{i\mu z} \cdot \mathbf{S}_{i\mu x} + \frac{1}{4} n_{i\mu z} n_{i\mu x} \right) \\
& + J_H \sum_{i\mu} \left(c_{i\mu z\uparrow}^\dagger c_{i\mu z\downarrow}^\dagger c_{i\mu x\downarrow} c_{i\mu x\uparrow} + \text{h.c.} \right).
\end{aligned} \tag{2}$$

Here, $\mathbf{S}_{i\mu\alpha} = \frac{1}{2} c_{i\mu\alpha\sigma}^\dagger [\boldsymbol{\sigma}]_{\sigma\sigma'} c_{i\mu\alpha\sigma'}$ is the spin operator with Pauli matrices $\boldsymbol{\sigma} = (\sigma_x, \sigma_y, \sigma_z)$. $n_{i\mu\alpha\sigma} = c_{i\mu\alpha\sigma}^\dagger c_{i\mu\alpha\sigma}$ is the particle occupancy number operator. U and V represent the onsite intra and interorbital Coulomb repulsions, respectively. The Hund's coupling J_H drives the d_{z^2} and $d_{x^2-y^2}$ electrons at the same site to form a spin triplet, as shown in Fig. 1(b). The condition of orbital rotational symmetry induces $U = V + 2J_H$ [97].

In the strong coupling limit, the large onsite Hubbard repulsion U forbids the formation of double occupancy for each orbital. When both the d_{z^2} and $d_{x^2-y^2}$ orbitals are single occupied on the same site, Hund's rule energetically favors the formation of an interorbital spin-triplet ($S = 1$) state. Considering these constraints, the relevant low-energy local Hilbert space at each site comprises eight possible configurations, depicted in Fig. 2.

Treating the kinetic hopping terms as perturbations to the dominant interaction terms, an effective low-energy Hamiltonian can be derived via the superexchange mechanism using standard second-order perturbation theory. This procedure yields an effective bilayer t - J type model that describes the dynamics of the allowed local states, including spin- $\frac{1}{2}$ singlons (single occupancy in either d_{z^2} or $d_{x^2-y^2}$) and spin-1 triplet doublons (single occupancy

in both orbitals). The resulting Hamiltonian is given by:

$$H = H_t + H_J^\parallel + H_J^\perp + V \sum_{i\mu\sigma\sigma'} n_{i\mu z\sigma} n_{i\mu x\sigma'} - 2J_H \sum_{i\mu} \left(\mathbf{S}_{i\mu z} \cdot \mathbf{S}_{i\mu x} + \frac{1}{4} n_{i\mu z} n_{i\mu x} \right), \quad (3)$$

where H_t represents the effective hopping terms (projected onto the restricted Hilbert space); H_J^\parallel and H_J^\perp contain the intralayer and interlayer superexchange interactions, respectively; The last two terms account for the interorbital Coulomb repulsion V and the Hund's coupling J_H , which influence the local energy of each configuration in Fig. 2.

The intralayer superexchange Hamiltonian takes the form:

$$\begin{aligned} H_J^\parallel = & \sum_{\langle ij \rangle \mu} J_{zz}^\parallel \left(\mathbf{S}_{i\mu z} \cdot \mathbf{S}_{j\mu z} - \frac{1}{4} n_{i\mu z} n_{j\mu z} \right) \\ & + \sum_{\langle ij \rangle \mu} J_{xx}^\parallel \left(\mathbf{S}_{i\mu x} \cdot \mathbf{S}_{j\mu x} - \frac{1}{4} n_{i\mu x} n_{j\mu x} \right) \\ & + \sum_{\langle ij \rangle \mu} J_{dd}^\parallel \left(\mathbf{S}_{i\mu d} \cdot \mathbf{S}_{j\mu d} - \frac{1}{4} n_{i\mu d} n_{j\mu d} \right) \\ & + \sum_{\langle ij \rangle \mu} J_{zx}^\parallel \left(\mathbf{S}_{i\mu z} \cdot \mathbf{S}_{j\mu x} - \frac{1}{4} n_{i\mu z} n_{j\mu x} + (i \leftrightarrow j) \right) \\ & + \sum_{\langle ij \rangle \mu} J_{zd}^\parallel \left(\mathbf{S}_{i\mu z} \cdot \mathbf{S}_{j\mu d} - \frac{1}{4} n_{i\mu z} n_{j\mu d} + (i \leftrightarrow j) \right) \\ & + \sum_{\langle ij \rangle \mu} J_{xd}^\parallel \left(\mathbf{S}_{i\mu x} \cdot \mathbf{S}_{j\mu d} - \frac{1}{4} n_{i\mu x} n_{j\mu d} + (i \leftrightarrow j) \right), \end{aligned} \quad (4)$$

and the interlayer superexchange Hamiltonian is:

$$\begin{aligned} H_J^\perp = & \sum_i J_{zz}^\perp \left(\mathbf{S}_{itz} \cdot \mathbf{S}_{ibz} - \frac{1}{4} n_{itz} n_{ibz} \right) \\ & + \sum_i J_{dd}^\perp \left(\mathbf{S}_{itd} \cdot \mathbf{S}_{ibd} - \frac{1}{4} n_{itd} n_{ibd} \right) \\ & + \sum_i J_{zx}^\perp \left(\mathbf{S}_{itz} \cdot \mathbf{S}_{ibx} - \frac{1}{4} n_{itz} n_{ibx} + (t \leftrightarrow b) \right) \\ & + \sum_i J_{zd}^\perp \left(\mathbf{S}_{itz} \cdot \mathbf{S}_{ibd} - \frac{1}{4} n_{itz} n_{ibd} + (t \leftrightarrow b) \right) \\ & + \sum_i J_{xd}^\perp \left(\mathbf{S}_{itx} \cdot \mathbf{S}_{ibd} - \frac{1}{4} n_{itx} n_{ibd} + (t \leftrightarrow b) \right). \end{aligned} \quad (5)$$

Here, $\mathbf{S}_{i\mu\alpha}$ (with $\alpha = z$ or x) represents the spin- $\frac{1}{2}$ operator when there is only one electron occupying the d_{z^2} or $d_{x^2-y^2}$ orbital, respectively. $n_{i\mu\alpha} = \sum_\sigma n_{i\mu\alpha\sigma}$ represents the total particle number of the α orbital at the site i in the layer μ . $\mathbf{S}_{i\mu d}$ represents the spin-1 operator under Hund's rule when both the d_{z^2} and $d_{x^2-y^2}$ orbitals are singly occupied, and $n_{i\mu d} = \sum_\alpha n_{i\mu\alpha}$ is the

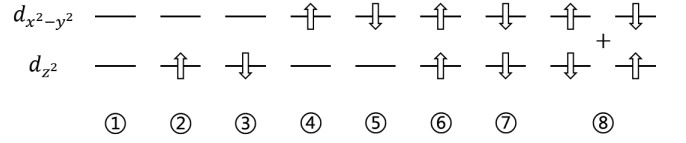


FIG. 2. The $3d^8$ configuration on each site with double holes, singlons and triplet doublons in the strong coupling limit.

total particle number of the site i in the layer μ under this occupation. The various superexchange parameters J quantify the effective antiferromagnetic spin couplings between different types of local states across NN bonds; for example, J_{zd}^\parallel describes the intralayer spin coupling between a d_{z^2} singlon and a triplet doublon. Explicit expressions relating these spin-exchange J parameters to the original Hubbard model parameters are provided in Appendix A.

We adopt data from the DFT calculations [32] as physical parameters for H_t . The intralayer hopping parameters are given by $t_{zz}^\parallel = 0.110$ eV, $t_{zx}^\parallel = 0.239$ eV and $t_{xx}^\parallel = 0.483$ eV. The interlayer hopping for the d_{z^2} orbital is $t_{zz}^\perp = 0.635$ eV, while the ones involving the $d_{x^2-y^2}$ orbital nearly vanish. The onsite energies are set to $\epsilon_z = 0.409$ eV and $\epsilon_x = 0.776$ eV. With the relationship of interaction strengths $U = V + 2J_H$ [97], the onsite Coulomb repulsion is chosen as $U = 5$ eV, and the Hund's coupling J_H ranges from $\frac{U}{8}$ to $\frac{U}{4}$ approximately.

III. SLAVE-PARTICLE MEAN-FIELD STUDY

In the slave-particle framework, the restriction to the physical Hilbert space can be systematically imposed. The fully empty state is defined as

$$|\text{empty}\rangle_{i\mu} = h_{i\mu}^\dagger |\text{vac}\rangle_{i\mu}, \quad (6)$$

where $|\text{vac}\rangle$ denotes the vacuum state for the slave particles, and the onsite energy of this empty state in the atomic limit is set to zero for simplicity.

The four singly-occupied states in Fig. 2 correspond to the spin- $\frac{1}{2}$ singlon configuration. To represent these states, we introduce a set of spinon operators

$$\begin{aligned} |\uparrow_z\rangle_{i\mu} &= b_{i\mu z\uparrow}^\dagger |\text{vac}\rangle_{i\mu}, & |\uparrow_x\rangle_{i\mu} &= b_{i\mu x\uparrow}^\dagger |\text{vac}\rangle_{i\mu}, \\ |\downarrow_z\rangle_{i\mu} &= b_{i\mu z\downarrow}^\dagger |\text{vac}\rangle_{i\mu}, & |\downarrow_x\rangle_{i\mu} &= b_{i\mu x\downarrow}^\dagger |\text{vac}\rangle_{i\mu}. \end{aligned} \quad (7)$$

Here, $b_{i\mu\alpha\sigma}^\dagger$ is a creation operator of bosonic spinon, acting on the vacuum state to generate the four spin- $\frac{1}{2}$ configurations. The corresponding spin- $\frac{1}{2}$ operators are defined in the conventional manner. For instance, the spin operator for a state with only the $d_{x^2-y^2}$ orbital occupied is given by $\mathbf{S}_{i\mu x} = \frac{1}{2} b_{i\mu x\sigma}^\dagger [\boldsymbol{\sigma}]_{\sigma\sigma'} b_{i\mu x\sigma'}$, where $\boldsymbol{\sigma} = (\sigma_x, \sigma_y, \sigma_z)$ are the Pauli matrices. The onsite energy of the single-occupied state in the d_{z^2} orbital is set

to zero, while for the $d_{x^2-y^2}$ orbital, a finite energy difference $\Delta_g = \epsilon_x - \epsilon_z$ is considered.

For the three spin-1 triplet doublers, we employ a three-component Schwinger fermion representation. The Schwinger fermion $f_{i\mu} = (f_{i\mu,+1}, f_{i\mu,0}, f_{i\mu,-1})^T$ labels each spin projection:

$$\begin{aligned} | + 1 \rangle_{i\mu} &= f_{i\mu,+1}^\dagger |\text{vac}\rangle_{i\mu}, \\ | 0 \rangle_{i\mu} &= f_{i\mu,0}^\dagger |\text{vac}\rangle_{i\mu}, \\ | - 1 \rangle_{i\mu} &= f_{i\mu,-1}^\dagger |\text{vac}\rangle_{i\mu}. \end{aligned} \quad (8)$$

The corresponding spin-1 operators are expressed as

$$\begin{aligned} \hat{S}_{i\mu d}^+ &= f_{i\mu}^\dagger S_+ f_{i\mu} = \sqrt{2}(f_{i\mu,+1}^\dagger f_{i\mu,0} + f_{i\mu,0}^\dagger f_{i\mu,-1}), \\ \hat{S}_{i\mu d}^- &= f_{i\mu}^\dagger S_- f_{i\mu} = \sqrt{2}(f_{i\mu,0}^\dagger f_{i\mu,+1} + f_{i\mu,-1}^\dagger f_{i\mu,0}), \\ \hat{S}_{i\mu d}^z &= f_{i\mu}^\dagger S_z f_{i\mu} = f_{i\mu,+1}^\dagger f_{i\mu,+1} - f_{i\mu,-1}^\dagger f_{i\mu,-1}, \end{aligned} \quad (9)$$

where the ladder operators are $\hat{S}_{i\mu}^\pm = \hat{S}_{i\mu}^x \pm i\hat{S}_{i\mu}^y$, and the matrices $\{S_+, S_-, S_z\}$ form the spin-1 irreducible representation of the SU(2) generators. The onsite energy of these spin-1 states is set to $V - J_H + \Delta_g$.

The original electron operators can be expressed in terms of these slave particle operators. For example, the creation operator for a $d_{x^2-y^2}$ -orbital electron at site i in layer μ with spin \uparrow is

$$c_{i\mu x\uparrow}^\dagger = f_{i\mu,+1}^\dagger b_{i\mu z\uparrow} + \frac{1}{\sqrt{2}} f_{i\mu,0}^\dagger b_{i\mu z\downarrow} + b_{i\mu x\uparrow}^\dagger h_{i\mu}, \quad (10)$$

with similar expressions for the spin- \downarrow state and the d_{z^2} orbital. To preserve fermionic statistics, we assign fermionic statistics to both f - and h -operators, while the b -operators are bosonic. The physical Hilbert space is further constrained by the following local condition

$$\begin{aligned} & b_{i\mu,+1}^\dagger b_{i\mu,+1} + b_{i\mu,0}^\dagger b_{i\mu,0} + b_{i\mu,-1}^\dagger b_{i\mu,-1} \\ & + h_{i\mu}^\dagger h_{i\mu} + f_{i\mu x\uparrow}^\dagger f_{i\mu x\uparrow} + f_{i\mu x\downarrow}^\dagger f_{i\mu x\downarrow} \\ & + f_{i\mu z\uparrow}^\dagger f_{i\mu z\uparrow} + f_{i\mu z\downarrow}^\dagger f_{i\mu z\downarrow} = 1, \end{aligned} \quad (11)$$

which corresponds to a local U(1) gauge symmetry associated with charge conservation.

A. Spin-1 Valence Bond Solid

When interlayer superexchange dominates, the two localized spin-triplet states along a rung tend to form a spin-1 singlet bond, as illustrated in Fig. 3. The corresponding rung spin-singlet pairing operator at lattice site j is given by

$$F_j^\dagger = \frac{1}{\sqrt{3}} \left(f_{jt,1}^\dagger f_{jb,-1}^\dagger - f_{jt,0}^\dagger f_{jb,0}^\dagger + f_{jt,-1}^\dagger f_{jb,1}^\dagger \right), \quad (12)$$

This describes the formation of a spin-1 singlet bond between neighboring sites jt and jb on a rung. In the

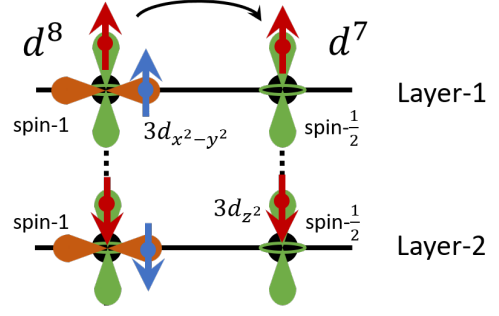


FIG. 3. Schematic diagram for the interlayer spin-1 singlet and spin- $\frac{1}{2}$ singlet.

mother $3d^8$ configuration, the system forms a spin-1 interlayer valence-bond solid (VBS) state, where the four electrons residing in the two E_g orbitals are strongly entangled, forming an interlayer spin singlet on each rung.

In the case of $\text{La}_3\text{Ni}_2\text{O}_7$, however, the actual electronic configuration is closer to $3d^{7.5}$, where additional holes prefer to occupy the $d_{x^2-y^2}$ orbitals. This emergence of SC in $\text{La}_3\text{Ni}_2\text{O}_7$ under pressure can be considered as doping the d^8 spin-1 VBS state. Upon doping, the spin-triplet configuration, characteristic of the $3d^8$ VBS, largely reduces to a $3d^7$ spin- $\frac{1}{2}$ configuration, predominantly involving the d_{z^2} orbital electron. As a result, the occupancy number of the spin-1 states, denoted n_1 , is approximately 0.5, and the occupancy number of the spin- $\frac{1}{2}$ states in the d_{z^2} orbital, n_z , is similarly around 0.5. Consequently, the strong interlayer exchange J_{zz}^\perp drives the formation of a spin- $\frac{1}{2}$ singlet bond along the rungs:

$$B_j^\dagger = \frac{1}{\sqrt{2}} \left(b_{jtz\uparrow}^\dagger b_{jbz\downarrow}^\dagger - b_{jtz\downarrow}^\dagger b_{jbz\uparrow}^\dagger \right), \quad (13)$$

where the $d_{x^2-y^2}$ orbital remains essentially empty on the rungs. This description captures the fundamental change in the electronic structure as the system transitions from a spin-1 to a spin- $\frac{1}{2}$ -dominated regime.

The nature of superconducting pairing in this doped spin-1 VBS state is fundamentally different from that of Cooper pairs in a Bardeen-Cooper-Schrieffer (BCS) superconductor [98]. In a conventional superconductor, the BCS wavefunction is a coherent superposition of the fully paired electron state and the vacuum (empty) state. In contrast, the exotic spinon pairing mechanism considered here involves a combination of two distinct singlets: one associated with spin- $\frac{1}{2}$ singlet states and the other with spin-1 singlet states. In the slave-particle formalism, this pairing can be represented as

$$|\text{spinon pair}\rangle = \prod_j \left(U_j B_j^\dagger + V_j F_j^\dagger \right) |\text{vac}\rangle, \quad (14)$$

where U_j , V_j are coefficients that reflect the relative weights of the two components. This mixed pairing structure reflects the complex interplay between spin-1 and

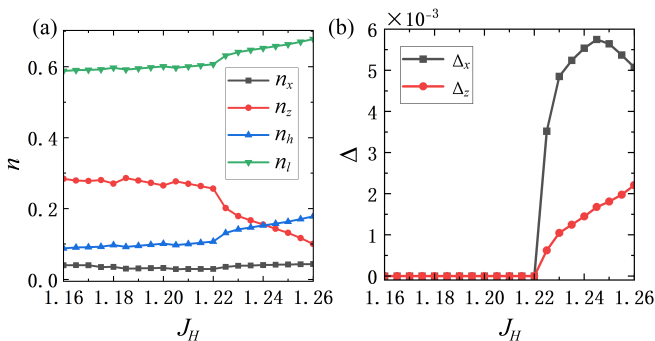


FIG. 4. Numerical results for (a) the densities and (b) pairing amplitude versus Hund's coupling J_H . The results indicate that an increase in J_H leads to a preference for electrons to occupy the spin-1 state, and also enhances interlayer pairing.

spin- $\frac{1}{2}$ physics in the doped system, and the resulting physical electron pairing emerges as a composite of these slave-particle pairings.

B. Numerical Results

Based on the preceding model analysis, we perform a slave-particle mean-field calculation to further clarify the physical picture described earlier. In the mean-field approach, we concentrate on the SC channel, where the terms $\mathbf{S}_z \cdot \mathbf{S}_d$ and $\mathbf{S}_x \cdot \mathbf{S}_d$ in Eq. 4 and 5 don't contribute. Additionally, we discard terms with negligible contributions for simplicity, including the intralayer $\mathbf{S}_z \cdot \mathbf{S}_z$ and $\mathbf{S}_z \cdot \mathbf{S}_x$, as well as interlayer $\mathbf{S}_x \cdot \mathbf{S}_x$ and $\mathbf{S}_z \cdot \mathbf{S}_x$. This allows us to focus more clearly on the behavior of onsite occupancy numbers and pairing amplitude as functions of the Hund's coupling J_H , and doping levels.

The calculated onsite occupancy numbers as a function of J_H are shown in Fig. 4(a). Here, n_l represents the onsite occupancy number for spin-1 state, while n_z and n_x correspond to the onsite occupancy numbers for the spin- $\frac{1}{2}$ states in the d_{z^2} and $d_{x^2-y^2}$ orbitals, respectively. Additionally, n_h denotes the occupancy of the empty state.

In the atomic limit, we would expect $n_l = n_z = 0.5$ and $n_x = n_h = 0$, reflecting equal occupancy of the spin-1 and spin- $\frac{1}{2}$ states. However, due to intraorbital hopping and interorbital hybridization, deviations from these atomic values are observed. As J_H increases, n_l and n_x tend to increase, whereas n_z decreases, indicating a shift in the balance between the spin-1 and spin- $\frac{1}{2}$ states as Hund's coupling strengthens. A pronounced change in occupancy numbers occurs near $J_H \approx 1.22$, suggesting a critical value in the electronic property. The sensitivity of the onsite occupancy numbers to J_H reflects the delicate balance between intraorbital and interorbital interactions in determining the electronic ground state.

The impact of this change is directly relevant to the behavior of superconducting pairing in the system.

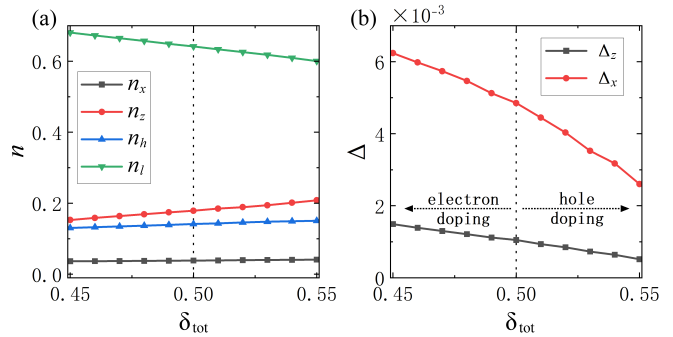


FIG. 5. Numerical results for (a) the densities and (b) pairing amplitude versus doping levels. The results show a positive correlation between the superconducting amplitude and the electron density.

Fig. 4(b) shows the J_H -dependence of the pairing amplitude for interlayer singlet pairing in the d_{z^2} and $d_{x^2-y^2}$ orbitals. As expected, pairing emerges rapidly with increasing J_H , with the interlayer pairing amplitude Δ_x dominating across the entire parameter range. This dominance of interlayer pairing originates from the robust interlayer spin-1 superexchange, which drives the formation of the rung pairs in this bilayer structure.

Additionally, the effect of doping on the system's electronic structure and pairing behavior is investigated, as illustrated in Fig. 5. The total hole density $\delta_{tot} = 0.5$ corresponds to the nominal $3d^{7.5}$ electronic configuration of Ni in the $\text{La}_3\text{Ni}_2\text{O}_7$. Hole doping ($\delta_{tot} > 0.5$) and electron doping (< 0.5) alter the occupancy numbers in distinct ways. As shown in Fig. 5(a), hole doping tends to reduce n_l , while increasing both increases n_x/n_z . Conversely, electron doping increases n_l , while decreasing n_x and n_z .

The superconducting pairing amplitude, shown in Fig. 5(b), exhibits a clear dependence on doping, with the interlayer $d_{x^2-y^2}$ pairing amplitude Δ_x remaining dominant across the full doping range. As hole doping increases, the pairing amplitude decreases, suggesting that hole doping weakens the overall superconducting state. In contrast, electron doping enhances the pairing amplitude.

IV. DENSITY MATRIX RENORMALIZATION GROUP STUDY

To further confirm the above picture, we employ the state-of-art DMRG method [95, 96] at zero temperature. The tensor libraries TensorKit [99] and FiniteMPS [100] provide an implementation of the required symmetry [101, 102]. We study the model on a ladder of $2 \times 1 \times L_x$ with the open boundary conditions in the x direction and choose the size $L_x = 96$ for calculations. We keep up to $D = 10000 \text{ U}(1)_{\text{charge}} \times \text{SU}(2)_{\text{spin}}$ multiplets in DMRG simulations and ensure the convergence accuracy of 10^{-8} .

To characterize the properties of ground states, we calculate the particle-number distribution of the two orbitals

$$\langle n_{i\alpha} \rangle = \frac{1}{2} \sum_{\mu\sigma} \langle n_{i\mu\alpha\sigma} \rangle, \quad (15)$$

and analyze various correlation functions. The single-particle Green's function is given by

$$G(r) = \frac{1}{4} \sum_{\mu\sigma} \left\langle \left(c_{i\mu z\sigma}^\dagger + c_{i\mu x\sigma} \right) \left(c_{i\mu z\sigma} + c_{i\mu x\sigma} \right) + \text{h.c.} \right\rangle, \quad (16)$$

where $r = |i - j|$ is the distance between the sites i and j . The charge density correlation function is defined as

$$D_\alpha(r) = \langle n_{i\alpha} n_{j\alpha} \rangle - \langle n_{i\alpha} \rangle \langle n_{j\alpha} \rangle, \quad (17)$$

and the spin-spin correlation function is

$$F(r) = \frac{1}{2} \sum_{\mu} \langle \mathbf{S}_{i\mu} \cdot \mathbf{S}_{j\mu} \rangle, \quad (18)$$

where \mathbf{S} is the total spin operator.

To characterize SC, we consider the possible pairing channels. The singlet pairing operators are given by

$$\begin{aligned} \Delta_{i\alpha}^{s,z\dagger} &= \frac{1}{\sqrt{2}} \left(c_{i\alpha\uparrow}^\dagger c_{i\beta\alpha\downarrow}^\dagger - c_{i\alpha\downarrow}^\dagger c_{i\beta\alpha\uparrow}^\dagger \right), \\ \Delta_{i\mu\alpha}^{s,x\dagger} &= \frac{1}{\sqrt{2}} \left(c_{i\mu\alpha\uparrow}^\dagger c_{i+1_x,\mu\alpha\downarrow}^\dagger - c_{i\mu\alpha\downarrow}^\dagger c_{i+1_x,\mu\alpha\uparrow}^\dagger \right), \end{aligned} \quad (19)$$

where the superscript s corresponds to singlet pairing and z and x correspond to interlayer pairing and intralayer pairing between the two NN sites in the x direction, respectively. Similarly, the triplet pairing operators are formulated as

$$\begin{aligned} \Delta_{i\alpha}^{t,z\dagger} &= c_{i\alpha\uparrow}^\dagger c_{i\beta\alpha\uparrow}^\dagger + c_{i\alpha\downarrow}^\dagger c_{i\beta\alpha\downarrow}^\dagger \\ &\quad + \frac{1}{\sqrt{2}} \left(c_{i\alpha\uparrow}^\dagger c_{i\beta\alpha\downarrow}^\dagger + c_{i\alpha\downarrow}^\dagger c_{i\beta\alpha\uparrow}^\dagger \right), \\ \Delta_{i\mu\alpha}^{t,x\dagger} &= c_{i\mu\alpha\uparrow}^\dagger c_{i+1_x,\mu\alpha\uparrow}^\dagger + c_{i\mu\alpha\downarrow}^\dagger c_{i+1_x,\mu\alpha\downarrow}^\dagger \\ &\quad + \frac{1}{\sqrt{2}} \left(c_{i\mu\alpha\uparrow}^\dagger c_{i+1_x,\mu\alpha\downarrow}^\dagger + c_{i\mu\alpha\downarrow}^\dagger c_{i+1_x,\mu\alpha\uparrow}^\dagger \right) \end{aligned} \quad (20)$$

In the numerical simulation, we measure the singlet pairing correlation functions

$$\begin{aligned} \Phi_\alpha^{s,zz}(r) &= \left\langle \Delta_{i\alpha}^{s,z\dagger} \Delta_{j\alpha}^{s,z} \right\rangle, \\ \Phi_\alpha^{s,xx}(r) &= \frac{1}{2} \sum_{\mu} \left\langle \Delta_{i\mu\alpha}^{s,x\dagger} \Delta_{j\mu\alpha}^{s,x} \right\rangle, \end{aligned} \quad (21)$$

The fitted Luttinger parameter K_{SC} negatively related to superconducting strength. Furthermore, the singlet pairing order parameters are defined as

$$\begin{aligned} \langle \Delta_\alpha^z \rangle &= \sqrt{\frac{1}{N_b} \sum_{i,j} \left\langle \Delta_{i\alpha}^{s,z\dagger} \Delta_{j\alpha}^{s,z} \right\rangle}, \\ \langle \Delta_\alpha^x \rangle &= \sqrt{\frac{1}{2N_b} \sum_{i,j,\mu} \left\langle \Delta_{i\mu\alpha}^{s,x\dagger} \Delta_{j\mu\alpha}^{s,x} \right\rangle}, \end{aligned} \quad (22)$$

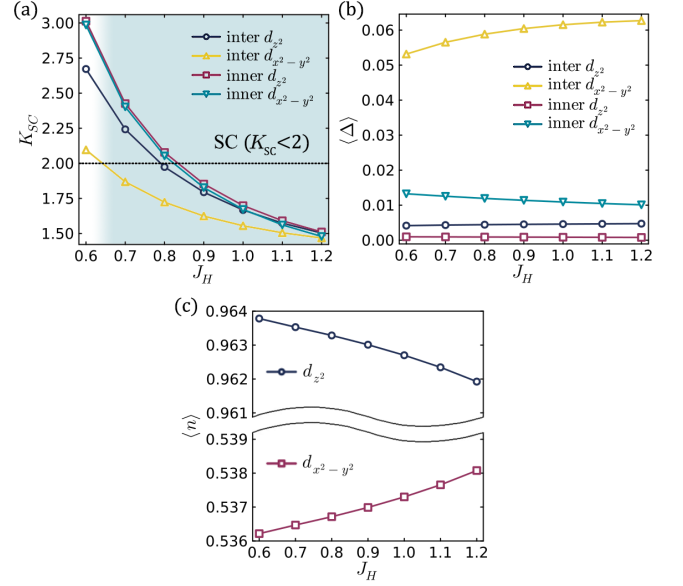


FIG. 6. (a) The Luttinger parameters K_{SC} of singlet pairing correlations $\Phi_\alpha^{s,zz}(r)$ and $\Phi_\alpha^{s,xx}(r)$ in the d_{z^2} and $d_{x^2-y^2}$ orbitals, with the Hund's coupling J_H . The legend *inter* and *inner* correspond to $\Phi_\alpha^{s,zz}(r)$ and $\Phi_\alpha^{s,xx}(r)$ respectively. (b) The singlet pairing order parameters $\langle \Delta_\alpha^z \rangle$ and $\langle \Delta_\alpha^x \rangle$. (c) The electron densities in the two E_g orbitals.

where i, j are restricted within $\frac{L_x}{4} \sim \frac{3L_x}{4}$ and N_b is the number of the credited pairs. Similarly, the triplet pairing correlation function takes the form of

$$\begin{aligned} \Phi_\alpha^{t,zz}(r) &= \left\langle \Delta_{i\alpha}^{t,z\dagger} \Delta_{j\alpha}^{t,z} \right\rangle, \\ \Phi_\alpha^{t,xx}(r) &= \frac{1}{2} \sum_{\mu} \left\langle \Delta_{i\mu\alpha}^{t,x\dagger} \Delta_{j\mu\alpha}^{t,x} \right\rangle, \end{aligned} \quad (23)$$

where the superscript t corresponds to triplet pairing.

We investigate the effect of Hund's coupling on SC and particle distribution. In Fig. 6(a), the emergence of the superconducting ($K_{\text{SC}} < 2$) corresponds to the region where $J_H \gtrsim 0.7$ eV. We observe that interlayer singlet pairing in the $d_{x^2-y^2}$ orbital remains dominant as J_H varies from 0.6 eV to 1.2 eV, with superconducting strength increasing monotonically alongside J_H . In the range of $J_H \gtrsim 1$, the difference between types of K_{SC} is insignificant, which may be due to the proximity effect. Thus we also calculate the order parameters $\langle \Delta_\alpha^z \rangle$ and $\langle \Delta_\alpha^x \rangle$ as shown in Fig. 6(b), further proving the dominance of interlayer $d_{x^2-y^2}$ orbital pairing. Fig. 6(c) illustrates that a higher J_H leads to an increased particle number in the $d_{x^2-y^2}$ orbital, which partially accounts for the enhanced SC by boosting carrier density.

Focusing on the typical case of $J_H = 1$ eV, we present additional detailed results in Fig. 7 and 8. Fig. 7(a) displays the particle number distribution on the two E_g orbitals. In Fig. 7(b) and (c), we illustrate the algebraic decay properties of the interlayer and intralayer singlet pairing correlation functions, suggesting that the

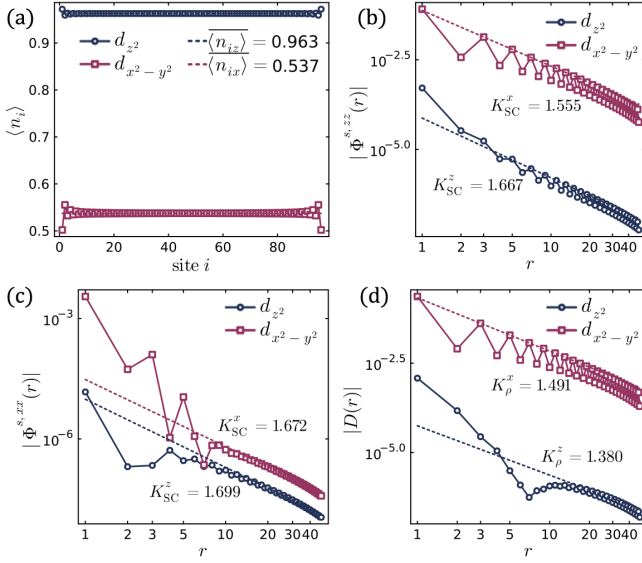


FIG. 7. (a) The electron densities in the two E_g orbitals. (b) shows the interlayer singlet pairing correlation functions of each orbital and (c) plots the intralayer singlet pairing correlation functions, both following an algebraic decay. (d) depicts the charge density correlation functions for each orbital, exhibiting algebraic decay.

quasi-one-dimensional system possesses characteristics of a Luther-Emery liquid [103]. Fig. 7(d) reveals that the charge correlation function follows an algebraic decay. This points to the possibility that the two-dimensional system may feature a mix of SC and charge density wave ordering, with interlayer electron pairing in the $d_{x^2-y^2}$ orbital as the primary source of SC.

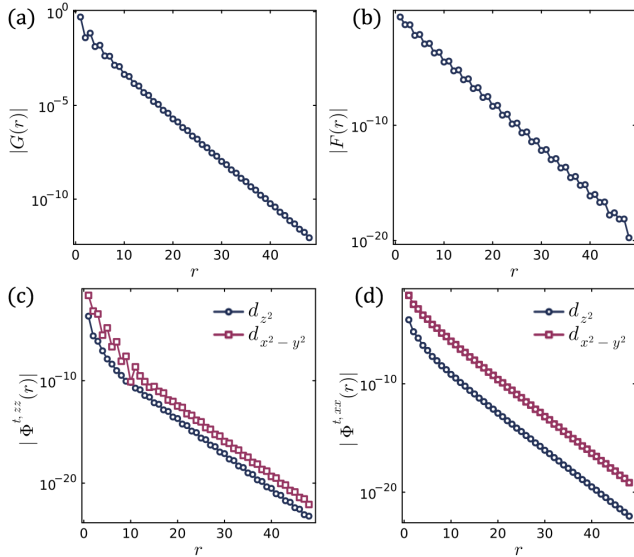


FIG. 8. (a) The Green's function, showing decay behavior. (b) The spin-spin correlation function. (c) displays the interlayer triplet pairing correlation functions across each orbital and (d) exhibits the intralayer triplet pairing correlation.

Both the Green's function shown in Fig. 8 and the spin correlation functions presented in Fig. 8(b) exhibit exponential decay. We also computed the interlayer and intralayer triplet pairing correlation functions, shown in Fig. 8(c) and (d), which both decay exponentially. These results suggest the absence of the corresponding order parameters in the pressurized $\text{La}_3\text{Ni}_2\text{O}_7$.

V. CONCLUSION AND DISCUSSION

In this work, we propose and study a bilayer two-orbital model for the superconducting $\text{La}_3\text{Ni}_2\text{O}_7$ under high pressure, which fully accounts for the effects of the onsite triplet doublons. The results presented here provide significant insight into the interplay between Hund's coupling, electron correlation, and SC in the bilayer nickelate material. The underlying mother state is formed within a strong-coupling regime, characterized by robust Hund's coupling that leads to spin-triplet configurations for the two E_g orbitals in the Ni $3d^8$ electronic state. The strong interlayer superexchange interactions promote the formation of interlayer spin-1 singlet states, resulting in an interlayer VBS structure. When the system approaches the physically relevant Ni $d^{7.5}$ valence in pressurized $\text{La}_3\text{Ni}_2\text{O}_7$, these spin-1 singlets gradually evolve into spin- $\frac{1}{2}$ singlets primarily involving the d_{z^2} orbitals. Doping introduces additional holes, which mediate phase coherence among these singlet bonds, eventually giving rise to SC.

The central finding of our work is the dominance of interlayer spinon singlet pairing across both the Hund's coupling (J_H) and doping regimes, suggesting that interlayer superexchange plays a pivotal role in stabilizing the superconducting state. This distinction points to the novelty of the superconducting mechanism in $\text{La}_3\text{Ni}_2\text{O}_7$, where the bilayer architecture, combined with the strong interlayer superexchange, offers a platform to explore unconventional SC. This structure fosters unique pairing mechanisms that rely heavily on the coupling between layers, distinguishing this system from the in-plane-dominated SC typically seen in cuprates and other layered systems.

Furthermore, our findings reveal that the coexistence of spin-1 and spin- $\frac{1}{2}$ singlets creates an unusual quantum entangled state that diverges from traditional models of SC. This entanglement between different spin channels suggests that both spin-1 and spin- $\frac{1}{2}$ singlets contribute to the overall pairing mechanism, raising fundamental questions about the precise nature of the superconducting phase in bilayer nickelates. The transition from a spin-1 valence bond solid to a mixed spin-1/spin- $\frac{1}{2}$ state, driven by doping, introduces the possibility of a rich and complex phase diagram. This phase diagram may exhibit a variety of superconducting properties that depend sensitively on parameters such as Hund's coupling, doping level, and orbital occupancy.

Note added: When finalizing the manuscript, we be-

come aware of a related preprint [77] that also considers an effective bilayer two-orbital t - J model incorporating strong Hund's coupling, similar to the model presented here. Our study builds upon such a model framework by performing detailed theoretical and numerical analyses (SPMF and DMRG) to investigate the nature of the SC pairing mechanism and symmetry.

ACKNOWLEDGMENTS

We are grateful to the stimulating discussions with Wei Li, Xing-Zhou Qu and Jialin Chen. C.W. is supported by the National Natural Science Foundation of China under the Grants No. 12234016 and No. 12174317. F.Y. is supported by the National Natural Science Foundation of China under the Grants No. 12074031. C.L. is supported by the National Natural Science Foundation of China under the Grants No. 12304180. This work has been supported by the New Cornerstone Science Foundation.

-
- [1] H. Sun, M. Huo, X. Hu, J. Li, Z. Liu, Y. Han, L. Tang, Z. Mao, P. Yang, B. Wang, J. Cheng, D.-X. Yao, G.-M. Zhang, and M. Wang, Signatures of superconductivity near 80K in a nickelate under high pressure, *Nature* **621**, 493 (2023).
- [2] Y. Zhang, D. Su, Y. Huang, Z. Shan, H. Sun, M. Huo, K. Ye, J. Zhang, Z. Yang, Y. Xu, Y. Su, R. Li, M. Smidman, M. Wang, L. Jiao, and H. Yuan, High-temperature superconductivity with zero resistance and strange-metal behaviour in $\text{La}_3\text{Ni}_2\text{O}_{7-\delta}$, *Nat. Phys.* **20**, 1269 (2024).
- [3] J. Hou, P.-T. Yang, Z.-Y. Liu, J.-Y. Li, P.-F. Shan, L. Ma, G. Wang, N.-N. Wang, H.-Z. Guo, J.-P. Sun, Y. Uwatoko, M. Wang, G.-M. Zhang, B.-S. Wang, and J.-G. Cheng, Emergence of high-temperature superconducting phase in pressurized $\text{La}_3\text{Ni}_2\text{O}_7$ crystals, *Chin. Phys. Lett.* **40**, 117302 (2023).
- [4] G. Wang, N. N. Wang, X. L. Shen, J. Hou, L. Ma, L. F. Shi, Z. A. Ren, Y. D. Gu, H. M. Ma, P. T. Yang, Z. Y. Liu, H. Z. Guo, J. P. Sun, G. M. Zhang, S. Calder, J.-Q. Yan, B. S. Wang, Y. Uwatoko, and J.-G. Cheng, Pressure-induced superconductivity in polycrystalline $\text{La}_3\text{Ni}_2\text{O}_7$, *Phys. Rev. X* **14**, 011040 (2024).
- [5] G. Wang, N. Wang, Y. Wang, L. Shi, X. Shen, J. Hou, H. Ma, P. Yang, Z. Liu, H. Zhang, X. Dong, J. Sun, B. Wang, K. Jiang, J. Hu, Y. Uwatoko, and J. Cheng, Observation of high-temperature superconductivity in the high-pressure tetragonal phase of $\text{La}_2\text{PrNi}_2\text{O}_{7-\delta}$, [arXiv:2311.08212](https://arxiv.org/abs/2311.08212) (2023).
- [6] M. Zhang, C. Pei, Q. Wang, Y. Zhao, C. Li, W. Cao, S. Zhu, J. Wu, and Y. Qi, Effects of pressure and doping on Ruddlesden-Popper phases $\text{La}_{n+1}\text{Ni}_n\text{O}_{3n+1}$, *J. Mater. Sci. Technol.* **185**, 147 (2024).
- [7] Y. Zhou, J. Guo, S. Cai, H. Sun, C. Li, J. Zhao, P. Wang, J. Han, X. Chen, Y. Chen, Q. Wu, Y. Ding, T. Xiang, H.-k. Mao, and L. Sun, Investigations of key issues on the reproducibility of high- T_c superconductivity emerging from compressed $\text{La}_3\text{Ni}_2\text{O}_7$, *Matter and Radiation at Extremes* **10**, 027801 (2025).
- [8] N. Wang, G. Wang, X. Shen, J. Hou, J. Luo, X. Ma, H. Yang, L. Shi, J. Dou, J. Feng, J. Yang, Y. Shi, Z. Ren, H. Ma, P. Yang, Z. Liu, Y. Liu, H. Zhang, X. Dong, Y. Wang, K. Jiang, J. Hu, S. Calder, J. Yan, J. Sun, B. Wang, R. Zhou, Y. Uwatoko, and J. Cheng, Bulk high-temperature superconductivity in the high-pressure tetragonal phase of bilayer $\text{La}_2\text{PrNi}_2\text{O}_7$, *Nature* **634**, 579 (2024).
- [9] J. Li, D. Peng, P. Ma, H. Zhang, Z. Xing, X. Huang, C. Huang, M. Huo, D. Hu, Z. Dong, X. Chen, T. Xie, H. Dong, H. Sun, Q. Zeng, H. Kwang Mao, and M. Wan, Identification of the superconductivity in bilayer nickelate $\text{La}_3\text{Ni}_2\text{O}_7$ upon 100 GPa, [arXiv:2404.11369](https://arxiv.org/abs/2404.11369) (2024).
- [10] Y. Ueki, H. Sakurai, H. Nagata, K. Yamane, R. Matsumoto, K. Terashima, K. Hirose, H. Ohta, M. Kato, and Y. Takano, Phase diagram of pressure-induced high temperature superconductor $\text{La}_3\text{Ni}_2\text{O}_{7+\delta}$, *J. Phys. Soc. Jpn.* **94**, 013703 (2025).
- [11] T. Fukamachi, Y. Kobayashi, T. Miyashita, and M. Sato, ^{139}La NMR studies of layered perovskite systems $\text{La}_3\text{Ni}_2\text{O}_{7-\delta}$ and $\text{La}_4\text{Ni}_3\text{O}_{10}$, *J. Phys. Chem. Solids* **62**, 195 (2001).
- [12] Z. Liu, H. Sun, M. Huo, X. Ma, Y. Ji, E. Yi, L. Li, H. Liu, J. Yu, Z. Zhang, Z. Chen, F. Liang, H. Dong, H. Guo, D. Zhong, B. Shen, S. Li, and M. Wang, Evidence for charge and spin density waves in single crystals of $\text{La}_3\text{Ni}_2\text{O}_7$ and $\text{La}_3\text{Ni}_2\text{O}_6$, *Sci. China-Phys. Mech. Astron.* **66**, 217411 (2023).
- [13] X. Chen, J. Choi, Z. Jiang, J. Mei, K. Jiang, J. Li, S. Agrestini, M. Garcia-Fernandez, X. Huang, H. Sun, D. Shen, M. Wang, J. Hu, Y. Lu, K.-J. Zhou, and D. Feng, Electronic and magnetic excitations in $\text{La}_3\text{Ni}_2\text{O}_7$, *Nat. Commun.* **15**, 9597 (2024).
- [14] M. Kakoi, T. Oi, Y. Ohshita, M. Yashima, K. Kuroki, T. Kato, H. Takahashi, S. Ishiwata, Y. Adachi, N. Hatada, T. Uda, and H. Mukuda, Multiband metallic ground state in multilayered nickelates $\text{La}_3\text{Ni}_2\text{O}_7$ and $\text{La}_4\text{Ni}_3\text{O}_{10}$ probed by ^{139}La -NMR at ambient pressure, *J. Phys. Soc. Jpn.* **93**, 053702 (2024).
- [15] T. Xie, M. Huo, X. Ni, F. Shen, X. Huang, H. Sun, H. C. Walker, D. Adroja, D. Yu, B. Shen, L. He, K. Cao, and M. Wang, Strong interlayer magnetic exchange coupling in $\text{La}_3\text{Ni}_2\text{O}_{7-\delta}$ revealed by inelastic neutron scattering, *Sci. Bull.* **69**, 3221 (2024).
- [16] N. K. Gupta, R. Gong, Y. Wu, M. Kang, C. T. Parzyck, B. Z. Gregory, N. Costa, R. Sutarto, S. Sarker, A. Singer, D. G. Schlom, K. M. Shen, and D. G. Hawthorn, Anisotropic spin stripe domains in bilayer $\text{La}_3\text{Ni}_2\text{O}_7$, [arXiv:2409.03210](https://arxiv.org/abs/2409.03210) (2024).
- [17] J.-J. Feng, T. Han, J.-P. Song, M.-S. Long, X.-Y. Hou, C.-J. Zhang, Q.-G. Mu, and L. Shan, Unaltered density wave transition and pressure-induced signature of superconductivity in Nd-doped $\text{La}_3\text{Ni}_2\text{O}_7$, *Phys. Rev. B* **110**, L100507 (2024).

- [18] Y. Meng, Y. Yang, H. Sun, S. Zhang, J. Luo, L. Chen, X. Ma, M. Wang, F. Hong, X. Wang, and X. Yu, Density-wave-like gap evolution in $\text{La}_3\text{Ni}_2\text{O}_7$ under high pressure revealed by ultrafast optical spectroscopy, *Nat. Commun.* **15**, 10408 (2024).
- [19] S. Fan, Z. Luo, M. Huo, Z. Wang, H. Li, H. Yang, M. Wang, D.-X. Yao, and H.-H. Wen, Tunneling spectra with gaplike features observed in nickelate $\text{La}_3\text{Ni}_2\text{O}_7$ at ambient pressure, *Phys. Rev. B* **110**, 134520 (2024).
- [20] M. Xu, G. C. Jose, A. Rutherford, H. Wang, S. Zhang, R. J. Cava, H. Zhou, W. Bi, and W. Xie, Pressure-induced phase transitions in bilayer $\text{La}_3\text{Ni}_2\text{O}_7$, [arXiv:2410.18840](https://arxiv.org/abs/2410.18840) (2024).
- [21] Y. Li, Y. Cao, L. Liu, P. Peng, H. Lin, C. Pei, M. Zhang, H. Wu, X. Du, W. Zhao, K. Zhai, X. Zhang, J. Zhao, M. Lin, P. Tan, Y. Qi, G. Li, H. Guo, L. Yang, and L. Yang, Distinct ultrafast dynamics of bilayer and trilayer nickelate superconductors regarding the density-wave-like transitions, *Sci. Bull.* **70**, 180 (2024).
- [22] Z. Liu, M. Huo, J. Li, Q. Li, Y. Liu, Y. Dai, X. Zhou, J. Hao, Y. Lu, M. Wang, and H.-H. Wen, Electronic correlations and partial gap in the bilayer nickelate $\text{La}_3\text{Ni}_2\text{O}_7$, *Nat. Commun.* **15**, 7570 (2024).
- [23] M. Wang, H.-H. Wen, T. Wu, D.-X. Yao, and T. Xiang, Normal and superconducting properties of $\text{La}_3\text{Ni}_2\text{O}_7$, *Chin. Phys. Lett.* **41**, 077402 (2024).
- [24] J. Yang, H. Sun, X. Hu, Y. Xie, T. Miao, H. Luo, H. Chen, B. Liang, W. Zhu, G. Qu, C.-Q. Chen, M. Huo, Y. Huang, S. Zhang, F. Zhang, F. Yang, Z. Wang, Q. Peng, H. Mao, G. Liu, Z. Xu, T. Qian, D.-X. Yao, M. Wang, L. Zhao, and X. J. Zhou, Orbital-dependent electron correlation in double-layer nickelate $\text{La}_3\text{Ni}_2\text{O}_7$, *Nat. Commun.* **15**, 4373 (2024).
- [25] Y. Li, X. Du, Y. Cao, C. Pei, M. Zhang, W. Zhao, K. Zhai, R. Xu, Z. Liu, Z. Li, J. Zhao, G. Li, Y. Qi, H. Guo, Y. Chen, and L. Yang, Electronic correlation and pseudogap-like behavior of high-temperature superconductor $\text{La}_3\text{Ni}_2\text{O}_7$, *Chin. Phys. Lett.* **41**, 087402 (2024).
- [26] M. Li, Y. Wang, C. Pei, M. Zhang, N. Li, J. Guan, M. Amboage, N.-D. Adama, Q. Kong, Y. Qi, and W. Yang, Distinguishing electronic band structure of single-layer and bilayer Ruddlesden-Popper nickelates probed by in-situ high pressure X-ray absorption near-edge spectroscopy, [arXiv:2410.04230](https://arxiv.org/abs/2410.04230) (2024).
- [27] Y. Liu, M. Ou, H. Chu, H. Yang, Q. Li, Y.-J. Zhang, and H.-H. Wen, Growth and characterization of the $\text{La}_3\text{Ni}_2\text{O}_{7-\delta}$ thin films: Dominant contribution of the $d_{x^2-y^2}$ orbital at ambient pressure, *Phys. Rev. Mater.* **8**, 124801 (2024).
- [28] K. Chen, X. Liu, J. Jiao, M. Zou, C. Jiang, X. Li, Y. Luo, Q. Wu, N. Zhang, Y. Guo, and L. Shu, Evidence of spin density waves in $\text{La}_3\text{Ni}_2\text{O}_{7-\delta}$, *Phys. Rev. Lett.* **132**, 256503 (2024).
- [29] R. Khasanov, T. J. Hicken, D. J. Gawryluk, V. Sazgari, I. Plokhikh, L. P. Sorel, M. Bartkowiak, S. Bötzel, F. Lechermann, I. M. Eremin, H. Luetkens, and Z. Guguchia, Pressure-enhanced splitting of density wave transitions in $\text{La}_3\text{Ni}_2\text{O}_{7-\delta}$, *Nature Physics* **21**, 430 (2025).
- [30] D. Zhao, Y. Zhou, M. Huo, Y. Wang, L. Nie, Y. Yang, J. Ying, M. Wang, T. Wu, and X. Chen, Pressure-enhanced spin-density-wave transition in double-layer nickelate $\text{La}_3\text{Ni}_2\text{O}_{7-\delta}$, *Science Bulletin* (2025).
- [31] B. Chen, H. Zhang, J. Li, D. Hu, M. Huo, S. Wang, C. Xi, Z. Wang, H. Sun, M. Wang, and B. Shen, Unveiling the multiband metallic nature of the normal state in the nickelate $\text{La}_3\text{Ni}_2\text{O}_7$, *Phys. Rev. B* **111**, 054519 (2025).
- [32] Z. Luo, X. Hu, M. Wang, W. Wú, and D.-X. Yao, Bilayer two-orbital model of $\text{La}_3\text{Ni}_2\text{O}_7$ under pressure, *Phys. Rev. Lett.* **131**, 126001 (2023).
- [33] Q.-G. Yang, D. Wang, and Q.-H. Wang, Possible S_{\pm} -wave superconductivity in $\text{La}_3\text{Ni}_2\text{O}_7$, *Phys. Rev. B* **108**, L140505 (2023).
- [34] V. Christiansson, F. Petocchi, and P. Werner, Correlated electronic structure of $\text{La}_3\text{Ni}_2\text{O}_7$ under pressure, *Phys. Rev. Lett.* **131**, 206501 (2023).
- [35] H. Oh and Y.-H. Zhang, Type-II t - J model and shared superexchange coupling from Hund's rule in superconducting $\text{La}_3\text{Ni}_2\text{O}_7$, *Phys. Rev. B* **108**, 174511 (2023).
- [36] X. Sui, X. Han, H. Jin, X. Chen, L. Qiao, X. Shao, and B. Huang, Electronic properties of the bilayer nickelates $\text{R}_3\text{Ni}_2\text{O}_7$ with oxygen vacancies (R=La or Ce), *Phys. Rev. B* **109**, 205156 (2024).
- [37] Y. Zhang, L.-F. Lin, A. Moreo, and E. Dagotto, Electronic structure, dimer physics, orbital-selective behavior, and magnetic tendencies in the bilayer nickelate superconductor $\text{La}_3\text{Ni}_2\text{O}_7$ under pressure, *Phys. Rev. B* **108**, L180510 (2023).
- [38] J. Huang, Z. D. Wang, and T. Zhou, Impurity and vortex states in the bilayer high-temperature superconductor $\text{La}_3\text{Ni}_2\text{O}_7$, *Phys. Rev. B* **108**, 174501 (2023).
- [39] Y. Shen, M. Qin, and G.-M. Zhang, Effective bilayer model hamiltonian and density-matrix renormalization group study for the high- T_c superconductivity $\text{La}_3\text{Ni}_2\text{O}_7$ under high pressure, *Chin. Phys. Lett.* **40**, 127401 (2023).
- [40] Y.-F. Yang, G.-M. Zhang, and F.-C. Zhang, Interlayer valence bonds and two-component theory for high- T_c superconductivity of $\text{La}_3\text{Ni}_2\text{O}_7$ under pressure, *Phys. Rev. B* **108**, L201108 (2023).
- [41] Q. Qin and Y.-F. Yang, High- T_c superconductivity by mobilizing local spin singlets and possible route to higher T_c in pressurized $\text{La}_3\text{Ni}_2\text{O}_7$, *Phys. Rev. B* **108**, L140504 (2023).
- [42] Y.-B. Liu, J.-W. Mei, F. Ye, W.-Q. Chen, and F. Yang, s^{\pm} -wave pairing and the destructive role of apical-oxygen deficiencies in $\text{La}_3\text{Ni}_2\text{O}_7$ under pressure, *Phys. Rev. Lett.* **131**, 236002 (2023).
- [43] F. Lechermann, J. Gondolf, S. Bötzel, and I. M. Eremin, Electronic correlations and superconducting instability in $\text{La}_3\text{Ni}_2\text{O}_7$ under high pressure, *Phys. Rev. B* **108**, L201121 (2023).
- [44] H. Sakakibara, N. Kitamine, M. Ochi, and K. Kuroki, Possible high T_c superconductivity in $\text{La}_3\text{Ni}_2\text{O}_7$ under high pressure through manifestation of a nearly half-filled bilayer Hubbard model, *Phys. Rev. Lett.* **132**, 106002 (2024).
- [45] Y. Gu, C. Le, Z. Yang, X. Wu, and J. Hu, Effective model and pairing tendency in bilayer Ni-based superconductor $\text{La}_3\text{Ni}_2\text{O}_7$, [arXiv:2306.07275](https://arxiv.org/abs/2306.07275) (2023).
- [46] C. Lu, Z. Pan, F. Yang, and C. Wu, Interlayer-coupling-driven high-temperature superconductivity in $\text{La}_3\text{Ni}_2\text{O}_7$ under pressure, *Phys. Rev. Lett.* **132**, 146002 (2024).
- [47] Z. Liao, L. Chen, G. Duan, Y. Wang, C. Liu, R. Yu, and Q. Si, Electron correlations and superconductivity in $\text{La}_3\text{Ni}_2\text{O}_7$ under pressure tuning, *Phys. Rev. B* **108**,

- 214522 (2023).
- [48] X.-Z. Qu, D.-W. Qu, J. Chen, C. Wu, F. Yang, W. Li, and G. Su, Bilayer t - J - J_{\perp} model and magnetically mediated pairing in the pressurized nickelate $\text{La}_3\text{Ni}_2\text{O}_7$, *Phys. Rev. Lett.* **132**, 036502 (2024).
- [49] K. Jiang, Z. Wang, and F.-C. Zhang, High temperature superconductivity in $\text{La}_3\text{Ni}_2\text{O}_7$, *Chin. Phys. Lett.* (2023).
- [50] Y. Zhang, L.-F. Lin, A. Moreo, T. A. Maier, and E. Dagotto, Trends in electronic structures and s_{\pm} -wave pairing for the rare-earth series in bilayer nickelate superconductor $R_3\text{Ni}_2\text{O}_7$, *Phys. Rev. B* **108**, 165141 (2023).
- [51] R. Jiang, J. Hou, Z. Fan, Z.-J. Lang, and W. Ku, Pressure driven fractionalization of ionic spins results in cupratelike high- T_c superconductivity in $\text{La}_3\text{Ni}_2\text{O}_7$, *Phys. Rev. Lett.* **132**, 126503 (2024).
- [52] D.-C. Lu, M. Li, Z.-Y. Zeng, W. Hou, J. Wang, F. Yang, and Y.-Z. You, Superconductivity from doping symmetric mass generation insulators: Application to $\text{La}_3\text{Ni}_2\text{O}_7$ under pressure, [arXiv:2308.11195](https://arxiv.org/abs/2308.11195) (2023).
- [53] N. Kitamine, M. Ochi, and K. Kuroki, Theoretical designing of multiband nickelate and palladate superconductors with $d^{8+\delta}$ configuration, [arXiv:2308.12750](https://arxiv.org/abs/2308.12750) (2023).
- [54] J.-X. Zhang, H.-K. Zhang, Y.-Z. You, and Z.-Y. Weng, Strong pairing originated from an emergent \mathbb{Z}_2 berry phase in $\text{La}_3\text{Ni}_2\text{O}_7$, *Phys. Rev. Lett.* **133**, 126501 (2024).
- [55] Z. Pan, C. Lu, F. Yang, and C. Wu, Effect of rare-earth element substitution in superconducting $R_3\text{Ni}_2\text{O}_7$ under pressure, *Chin. Phys. Lett.* **41**, 087401 (2024).
- [56] H. Sakakibara, M. Ochi, H. Nagata, Y. Ueki, H. Sakurai, R. Matsumoto, K. Terashima, K. Hirose, H. Ohta, M. Kato, Y. Takano, and K. Kuroki, Theoretical analysis on the possibility of superconductivity in the trilayer Ruddlesden-Popper nickelate $\text{La}_4\text{Ni}_3\text{O}_{10}$ under pressure and its experimental examination: Comparison with $\text{La}_3\text{Ni}_2\text{O}_7$, *Phys. Rev. B* **109**, 144511 (2024).
- [57] H. Lange, L. Homeier, E. Demler, U. Schollwöck, A. Bohrdt, and F. Grusdt, Pairing dome from an emergent feshbach resonance in a strongly repulsive bilayer model, *Phys. Rev. B* **110**, L081113 (2024).
- [58] H. Yang, H. Oh, and Y.-H. Zhang, Strong pairing from a small Fermi surface beyond weak coupling: Application to $\text{La}_3\text{Ni}_2\text{O}_7$, *Phys. Rev. B* **110**, 104517 (2024).
- [59] H. Lange, L. Homeier, E. Demler, U. Schollwöck, F. Grusdt, and A. Bohrdt, Feshbach resonance in a strongly repulsive ladder of mixed dimensionality: A possible scenario for bilayer nickelate superconductors, *Phys. Rev. B* **109**, 045127 (2024).
- [60] Z. Fan, J.-F. Zhang, B. Zhan, D. Lv, X.-Y. Jiang, B. Normand, and T. Xiang, Superconductivity in nickelate and cuprate superconductors with strong bilayer coupling, *Phys. Rev. B* **110**, 024514 (2024).
- [61] Y. Cao and Y.-f. Yang, Flat bands promoted by Hund's rule coupling in the candidate double-layer high-temperature superconductor $\text{La}_3\text{Ni}_2\text{O}_7$ under high pressure, *Phys. Rev. B* **109**, L081105 (2024).
- [62] Y. Zhang, L.-F. Lin, A. Moreo, T. A. Maier, and E. Dagotto, Structural phase transition, s_{\pm} -wave pairing, and magnetic stripe order in bilayered superconductor $\text{La}_3\text{Ni}_2\text{O}_7$ under pressure, *Nat. Commun.* **15**, 2470 (2024).
- [63] B. Geisler, J. J. Hamlin, G. R. Stewart, R. G. Hennig, and P. Hirschfeld, Structural transitions, octahedral rotations, and electronic properties of $A_3\text{Ni}_2\text{O}_7$ rare-earth nickelates under high pressure, *npj Quantum Mater.* **9**, 38 (2024).
- [64] L. C. Rhodes and P. Wahl, Structural routes to stabilize superconducting $\text{La}_3\text{Ni}_2\text{O}_7$ at ambient pressure, *Phys. Rev. Mater.* **8**, 044801 (2024).
- [65] Y. Zhang, L.-F. Lin, A. Moreo, T. A. Maier, and E. Dagotto, Electronic structure, magnetic correlations, and superconducting pairing in the reduced Ruddlesden-Popper bilayer $\text{La}_3\text{Ni}_2\text{O}_6$ under pressure: Different role of $d_{3z^2-r^2}$ orbital compared with $\text{La}_3\text{Ni}_2\text{O}_7$, *Phys. Rev. B* **109**, 045151 (2024).
- [66] B. Geisler, L. Fanfarillo, J. J. Hamlin, G. R. Stewart, R. G. Hennig, and P. J. Hirschfeld, Optical properties and electronic correlations in $\text{La}_3\text{Ni}_2\text{O}_{7-\delta}$ bilayer nickelates under high pressure, *npj Quantum Mater.* **9**, 89 (2024).
- [67] Y.-H. Tian, Y. Chen, J.-M. Wang, R.-Q. He, and Z.-Y. Lu, Correlation effects and concomitant two-orbital s_{\pm} -wave superconductivity in $\text{La}_3\text{Ni}_2\text{O}_7$ under high pressure, *Phys. Rev. B* **109**, 165154 (2024).
- [68] Z. Luo, B. Lv, M. Wang, W. Wú, and D.-X. Yao, High- T_c superconductivity in $\text{La}_3\text{Ni}_2\text{O}_7$ based on the bilayer two-orbital t-J model, *npj Quantum Mater.* **9**, 61 (2024).
- [69] T. Kaneko, H. Sakakibara, M. Ochi, and K. Kuroki, Pair correlations in the two-orbital Hubbard ladder: Implications for superconductivity in the bilayer nickelate $\text{La}_3\text{Ni}_2\text{O}_7$, *Phys. Rev. B* **109**, 045154 (2024).
- [70] Y.-F. Yang, Decomposition of multilayer superconductivity with interlayer pairing, *Phys. Rev. B* **110**, 104507 (2024).
- [71] C. Lu, Z. Pan, F. Yang, and C. Wu, Interplay of two E_g orbitals in superconducting $\text{La}_3\text{Ni}_2\text{O}_7$ under pressure, *Phys. Rev. B* **110**, 094509 (2024).
- [72] Z. Ouyang, M. Gao, and Z.-Y. Lu, Absence of electron-phonon coupling superconductivity in the bilayer phase of $\text{La}_3\text{Ni}_2\text{O}_7$ under pressure, *npj Quantum Mater.* **9**, 80 (2024).
- [73] X. Wu, H. Yang, and Y.-H. Zhang, Deconfined Fermi liquid to Fermi liquid transition and superconducting instability, *Phys. Rev. B* **110**, 125122 (2024).
- [74] Y. Zhang, L.-F. Lin, A. Moreo, T. A. Maier, and E. Dagotto, Electronic structure, self-doping, and superconducting instability in the alternating single-layer trilayer stacking nickelates $\text{La}_3\text{Ni}_2\text{O}_7$, *Phys. Rev. B* **110**, L060510 (2024).
- [75] S. Ryeong, N. Witt, and T. O. Wehling, Quenched pair breaking by interlayer correlations as a key to superconductivity in $\text{La}_3\text{Ni}_2\text{O}_7$, *Phys. Rev. Lett.* **133**, 096002 (2024).
- [76] Y. Wang, Z. Chen, Y. Zhang, K. Jiang, and J. Hu, The Mottness and the Anderson localization in bilayer nickelate $\text{La}_3\text{Ni}_2\text{O}_{7-\delta}$, [arXiv:2501.08536](https://arxiv.org/abs/2501.08536) (2025).
- [77] T. Kaneko, M. Kakoi, and K. Kuroki, t - J model for strongly correlated two-orbital systems: Application to bilayer nickelate superconductors, [arxiv:2504.10114](https://arxiv.org/abs/2504.10114) (2025).
- [78] E. K. Ko, Y. Yu, Y. Liu, L. Bhatt, J. Li, V. Thampy, C.-T. Kuo, B. Y. Wang, Y. Lee, K. Lee, J.-S. Lee, B. H. Goodge, D. A. Muller, and H. Y. Hwang, Signatures of ambient pressure superconductivity in thin

- film $\text{La}_3\text{Ni}_2\text{O}_7$, *Nature* **638**, 935 (2024).
- [79] G. Zhou, W. Lv, H. Wang, Z. Nie, Y. Chen, Y. Li, H. Huang, W. Chen, Y.-J. Sun, Q.-K. Xue, and Z. Chen, Ambient-pressure superconductivity onset above 40 K in $(\text{La,Pr})_3\text{Ni}_2\text{O}_7$ films, *Nature* (2025).
- [80] Y. Liu, E. K. Ko, Y. Tarn, L. Bhatt, B. H. Goodge, D. A. Muller, S. Raghu, Y. Yu, and H. Y. Hwang, Superconductivity and normal-state transport in compressively strained $\text{La}_2\text{PrNi}_2\text{O}_7$ thin films, [arXiv:2501.08022](https://arxiv.org/abs/2501.08022) (2025).
- [81] L. Bhatt, A. Y. Jiang, E. K. Ko, N. Schnitzer, G. A. Pan, D. F. Segedin, Y. Liu, Y. Yu, Y.-F. Zhao, E. A. Morales, C. M. Brooks, A. S. Botana, H. Y. Hwang, J. A. Mundy, D. A. Muller, and B. H. Goodge, Resolving structural origins for superconductivity in strain-engineered $\text{La}_3\text{Ni}_2\text{O}_7$ thin films, [arXiv:2501.08204](https://arxiv.org/abs/2501.08204) (2025).
- [82] C. Yue, J.-J. Miao, H. Huang, Y. Hua, P. Li, Y. Li, G. Zhou, W. Lv, Q. Yang, H. Sun, Y.-J. Sun, J. Lin, Q.-K. Xue, Z. Chen, and W.-Q. Chen, Correlated electronic structures and unconventional superconductivity in bilayer nickelate heterostructures, [arXiv:2501.06875](https://arxiv.org/abs/2501.06875) (2025).
- [83] Z.-Y. Shao, Y.-B. Liu, M. Liu, and F. Yang, Band structure and pairing nature of $\text{La}_3\text{Ni}_2\text{O}_7$ thin film at ambient pressure, [arXiv:2501.10409](https://arxiv.org/abs/2501.10409) (2025).
- [84] X. Hu, W. Qiu, C.-Q. Chen, Z. Luo, and D.-X. Yao, Electronic structures and multi-orbital models of $\text{La}_3\text{Ni}_2\text{O}_7$ thin films, [arXiv:2503.17223](https://arxiv.org/abs/2503.17223) (2025).
- [85] C. Tsuei and J. Kirtley, Pairing symmetry in cuprate superconductors, *Rev. Mod. Phys.* **72**, 969 (2000).
- [86] P. A. Lee, N. Nagaosa, and X.-G. Wen, Doping a Mott insulator: Physics of high-temperature superconductivity, *Rev. Mod. Phys.* **78**, 17 (2006).
- [87] L. Taillefer, Scattering and pairing in cuprate superconductors, *Annu. Rev. Condens. Matter Phys.* **1**, 51 (2010).
- [88] C. Proust and L. Taillefer, The remarkable underlying ground states of cuprate superconductors, *Ann. Rev. Condens. Matter Phys.* **10**, 409 (2019).
- [89] A. S. Botana and M. R. Norman, Similarities and differences between LaNiO_2 and CaCuO_2 and implications for superconductivity, *Phys. Rev. X* **10**, 011024 (2020).
- [90] F. Zhang and T. Rice, Effective hamiltonian for the superconducting Cu oxides, *Phys. Rev. B* **37**, 3759 (1988).
- [91] D. Li, K. Lee, B. Y. Wang, M. Osada, S. Crossley, H. R. Lee, Y. Cui, Y. Hikita, and H. Y. Hwang, Superconductivity in an infinite-layer nickelate, *Nature* **572**, 624 (2019).
- [92] Y. Nomura and R. Arita, Superconductivity in infinite-layer nickelates, *Rep. Prog. Phys.* **85**, 052501 (2022).
- [93] B. Y. Wang, K. Lee, and B. H. Goodge, Experimental progress in superconducting nickelates, *Ann. Rev. Condens. Matter Phys.* **15** (2024).
- [94] G. Kotliar and J. Liu, Superexchange mechanism and d -wave superconductivity, *Phys. Rev. B* **38**, 5142 (1988).
- [95] S. R. White, Density-matrix algorithms for quantum renormalization groups, *Phys. Rev. B* **48**, 10345 (1993).
- [96] Y. L. Lee, Y. W. Lee, C.-Y. Mou, and Z. Y. Weng, Two-leg t-J ladder: A mean-field description, *Phys. Rev. B* **60**, 13418 (1999).
- [97] C. Castellani, C. R. Natoli, and J. Ranninger, Magnetic structure of V_2O_3 in the insulating phase, *Phys. Rev. B* **18**, 4945 (1978).
- [98] M. Tinkham, *Introduction to superconductivity* (Courier Corporation, 2004).
- [99] Jutho, L. Devos, M. Hauru, maartenvd, ho oto, Gertian, L. Burgelman, tangwei94, J. TagBot, S. Carlström, V. Vanthilt, Xiaoyu, and qmortier, [Jutho/tensorkit.jl: v0.12.7](https://github.com/Jutho/tensorkit.jl) (2024).
- [100] Q. Li, [FiniteMPS.jl](https://github.com/qmli/FiniteMPS.jl) (2025).
- [101] A. Weichselbaum, Non-abelian symmetries in tensor networks: A quantum symmetry space approach, *Ann. Phys.* **327**, 2972 (2012).
- [102] A. Weichselbaum, X-symbols for non-abelian symmetries in tensor networks, *Phys. Rev. Res.* **2**, 023385 (2020).
- [103] A. Luther and V. J. Emery, Backward scattering in the one-dimensional electron gas, *Phys. Rev. Lett.* **33**, 589 (1974).

Appendix A: Details on the bilayer $t - J - J_H$ model

In the second-order perturbation theory, the electron interactions are treated as zero-order terms, while the kinetic terms are considered as first-order perturbations. The zero-order energies of some typical two-orbital configurations are shown in Fig. A1.

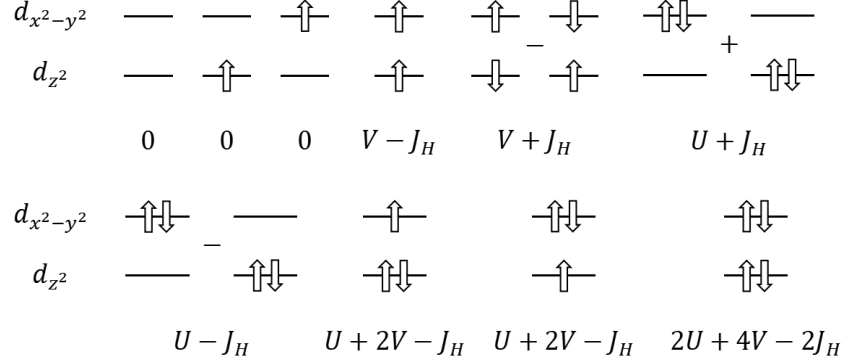


FIG. A1. The zero-order energies and the corresponding typical two-orbital configurations.

Near the natural filling of $\text{La}_3\text{Ni}_2\text{O}_7$, the local Hilbert space at each site is constrained to the d^8 configuration shown in Fig. 2 in the strong correlation limit. The effects of the discarded high-energy subspace are captured through the superexchange terms, whose strength is determined by second-order perturbation theory. The intralayer superexchange parameters of the bilayer $t - J - J_H$ model are related to the parameters of the original two-band Hubbard model through the following equations

$$\begin{aligned}
J_{zz}^{\parallel} &= \frac{4t_{zz}^{\parallel 2}}{U} + \frac{2t_{zx}^{\parallel 2}}{V + J_H + \epsilon_x - \epsilon_z}, \quad J_{xx}^{\parallel} = \frac{4t_{xx}^{\parallel 2}}{U} + \frac{2t_{zx}^{\parallel 2}}{V + J_H + \epsilon_z - \epsilon_x}, \\
J_{dd}^{\parallel} &= \frac{t_{zz}^{\parallel 2} + t_{xx}^{\parallel 2}}{U + J_H} + t_{zx}^{\parallel 2} \left[\frac{1}{U + J_H + \epsilon_z - \epsilon_x} + \frac{1}{U + J_H + \epsilon_x - \epsilon_z} \right], \\
J_{zx}^{\parallel} &= \frac{t_{zz}^{\parallel 2} + t_{xx}^{\parallel 2}}{V + J_H} + 2t_{zx}^{\parallel 2} \left[\frac{1}{U + \epsilon_z - \epsilon_x} + \frac{1}{U + \epsilon_x - \epsilon_z} \right], \\
J_{zd}^{\parallel} &= t_{zz}^{\parallel 2} \left[\frac{1}{U + V} + \frac{1}{U - V + J_H} \right] + \frac{t_{xx}^{\parallel 2}}{4J_H} + \frac{t_{zx}^{\parallel 2}}{2} \frac{1}{2J_H + \epsilon_x - \epsilon_z} \\
&\quad + t_{zx}^{\parallel 2} \left[\frac{1}{U + V + \epsilon_x - \epsilon_z} + \frac{1}{U - V + J_H + \epsilon_z - \epsilon_x} \right], \\
J_{xd}^{\parallel} &= t_{xx}^{\parallel 2} \left[\frac{1}{U + V} + \frac{1}{U - V + J_H} \right] + \frac{t_{zz}^{\parallel 2}}{4J_H} + \frac{t_{zx}^{\parallel 2}}{2} \frac{1}{2J_H + \epsilon_z - \epsilon_x} \\
&\quad + t_{zx}^{\parallel 2} \left[\frac{1}{U + V + \epsilon_z - \epsilon_x} + \frac{1}{U - V + J_H + \epsilon_x - \epsilon_z} \right],
\end{aligned} \tag{S1}$$

and the interlayer parameters are as follows

$$J_{zz}^{\perp} = \frac{4t_{zz}^{\perp 2}}{U}, \quad J_{dd}^{\perp} = \frac{t_{zz}^{\perp 2}}{U + J_H}, \quad J_{zx}^{\perp} = \frac{t_{zz}^{\perp 2}}{V + J_H}, \quad J_{zd}^{\perp} = t_{zz}^{\perp 2} \left[\frac{1}{U + V} + \frac{1}{U - V + J_H} \right], \quad J_{xd}^{\perp} = \frac{t_{zz}^{\perp 2}}{4J_H}. \tag{S2}$$

Particularly, the exclusion of the hole state results in the emergence of ferromagnetic interaction terms taking the form $-\frac{t^2}{V - J_H + \Delta\epsilon}$ in certain components of J . This is one of critical reasons for retaining it.